Plate tephra; preserved bubble walls from large slug bursts during violent Strombolian eruptions.

Citation for published version:
Ruth, D & Calder, E 2014, 'Plate tephra; preserved bubble walls from large slug bursts during violent Strombolian eruptions.', *Geology*, vol. 42, no. 1, pp. 11-44. https://doi.org/10.1130/G34859.1

Digital Object Identifier (DOI):
10.1130/G34859.1

Published In:
Geology

Publisher: GSA
Journal: GEOL: Geology
Article ID: G34859

Plate tephra: Preserved bubble walls from large slug bursts during violent Strombolian eruptions

Dawn C.S. Ruth[1]* and Eliza S. Calder[1,2]

[1]Department of Geology, 411 Cooke Hall, Buffalo, New York 14260, USA

[2]School of Geosciences, Grant Institute, The King's Buildings, West Mains Road, University of Edinburgh, Edinburgh EH9 3JW, UK

*E-mail: dcs34@buffalo.edu.

ABSTRACT

Unusual "plate tephra" are described and provide key information about rarely observed processes occurring during volcanic eruptions. The tephra formed during the 2008–2009 eruption of Llaima volcano, Chile and dispersed as far as 9 km from the vent. The plates are angular clasts of vesicular basaltic-andesite ranging in size from 1 to 14 cm and in thickness from 2 to 5 mm. External features such as ridges, varying degrees of curvature, and adhered material are present. Internal textures include strong crystal alignment and deformed enclaves. We propose that the plates are wall fragments formed during the rupture of large gas slugs associated with unsteady fire fountaining during the violent Strombolian phase of the eruption. The presence of plate tephra may be a diagnostic feature of highly unsteady activity where slug rupture is concurrent with the formation of a sustained eruption column.

INTRODUCTION

Distinct vesicular, basaltic andesite plates produced during the violent Strombolian opening phase of the 2008–2009 eruption of Llaima volcano, Chile, are investigated. These clasts are part of the juvenile tephra that also included a bimodal scoria population, characterized by brown and black scoria of low and high density, respectively. The plates share morphological characteristics with other unusual tephra such as pajaritos (Foshag and González, 1956), lava flakes (Maleyev and Vande-Kirkov, 1983), and limu o Pele (Schipper and White, 2010). Here we characterize the Llaima plate tephra, investigate their origin, and present a formation model that explains their morphological, textural, and dispersal characteristics. These plates represent an overlooked fragmentation product in the context of violent Strombolian eruptions, yet their generation has important implications for both conduit and plume processes.

2008–2009 ERUPTION OF LLAIMA

Llaima is a basaltic andesite stratovolcano (3125 m a.s.l. [above sea level]) located in the Southern Volcanic Zone of the Chilean Andes (Fig. 1), which erupted on average every 5–6 yr over the past 400 yr (Dzierma and Wehrmann, 2010). The latest eruption began on 1 January 2008 with violent Strombolian activity producing a sustained eruption column 3.5–11 km in height. A tephra blanket was deposited to the east-southeast, with thicknesses up to 11 cm (Smithsonian Institution, 2013a). The opening phase lasted 13.5 h, and lower level activity continued occasionally until 21 February 2008. Periodic low-level Strombolian activity persisted until July 2008 and waned by the end of April 2009 (Smithsonian Institution, 2013b).

DEPOSIT DESCRIPTION

Isopleth and isopach maps were produced for the tephra deposit (Fig. 2). For both scoria, the isopleth dispersal axis is due east of the vent, whereas the plate isopleths mark a more constrained zone to the east-southeast of the vent. Plate dimensions range from major axis diameters of ~14 cm (6 km from the vent) to 1 cm (9 km from the vent). Over the same area, black scoria range in size from 8 to 5 cm and the brown scoria from 7 to 3 cm (see the GSA Data Repository[1]). Plate abundance is estimated at <1% of the deposit by volume. It was not possible to distinguish whether they occupied a specific stratigraphic position.

The average plate density is 813 kg m^{-3}, whereas black and brown scoria densities are 583 kg m^{-3}, and 340 kg m^{-3}, respectively (Fig. 2a-c, insets). Eruption parameters were calculated as follows: the deposit volume is ~1.31×10^6 m^3 after Bonadonna and Costa (2012); and assuming a deposit density of 583 kg m^{-3}, the mass eruption rate (MER) for the opening 13 h, 36 min, is ~1.6×10^4 kg s^{-1} after Pioli et al. (2008).

TEPHRA CHARACTERISTICS

Hand Sample Textures

Plate shapes are oblate to bladed based on the Zingg shape parameter (Zingg, 1935; Wilson and Huang, 1979) (Fig. 3a) (Table 1). Minor axis dimensions are relatively constant (~4 mm), irrespective of plate size. By contrast, both scoria are generally equant to prolate. Approximately 90% of the 120 plates collected show curvature (Figs. 3b and 3c), but ~5% are folded with the edges tacked together. Scoria fragments are found adhered to either surface. Major-axis parallel ridges and tension cracks are present on the plate surfaces, occasionally on both sides.

Microscopic Textures

Thin sections show contrasting vesicularity and crystallinity for the three clast types (see the Data Repository, Fig. 4). Vesicularity in the black scoria is moderate to high with a few large, convolute vesicles whereas the brown scoria has very high vesicularity with abundant smaller, more homogeneous and rounded vesicles. In the plates, vesicles are convolute (with roughness from impinging crystals) to rounded and are well connected, often forming long trains of bubbles parallel to the major plane.

The black scoria are highly crystalline (~50%–60%; tachylite), whereas the brown scoria has lower crystallinity (~10%–15%; sideromelane). Some brown scoria contain clots of higher crystallinity magma which are similar to the black scoria. Crystallinity of the plates ranges from 40 to 50 vol%, similar to that observed in the black scoria. The black and brown scoria are texturally akin to the "high porphyricity" (HP) and "low porphyricity" (LP) scoria at Stromboli, respectively (Francalanci et al., 2004).

In all tephra, the mineralogy is mostly plagioclase with minor olivine (Fig. 4a and 4b). Plagioclase phenocrysts are 10–15 vol% of the overall crystal population, are euhedral to subhedral, sieve textured with growth rims, and occasionally occur as glomerocrysts. Olivine represent ~1 vol% of the total crystal population are subhedral to anhedral with visible melt inclusions. The groundmass for all tephra is mostly plagioclase microlites. Minor amounts of pyroxene and Fe-Ti spinel (<10 μm) are present in the black scoria and plates.

A striking internal textural feature unique to the plates is the ubiquitous alignment of crystals (Fig. 4c). Plagioclase and olivine phenocrysts and plagioclase microlites are parallel to subparallel to the plate-parallel plane. Relatively large, dark enclaves, with high Fe-Ti spinel and pyroxene content, are also present (Figs. 4a and 4b). The enclaves are aligned relative to the major plane and show pinch-and-swell features. Neighboring crystals and spinel-rich bands bend around the enclaves and glomerocrysts where present.

SIMILAR TEPHRA FROM ELSEWHERE

Similar tephra have been found elsewhere including pajaritos from Parícutin, Mexico (Foshag and González, 1956; Pioli et al., 2008) and lava flakes from Tolbachik, Russia (Maleyev and Vande-Kirkov, 1983). Pajaritos are microvesicular sideromelane plates, centimeteres in diameter that show partial folding, and have external millimeter size ridges (Pioli et al., 2008). Lava flakes are 5–20 cm diameter, 1–3 mm thick, slightly vesicular, and show deformation (Maleyev and Vande-Kirkov, 1983). Only Maleyev and Vande-Kirkov (1983) proposed that the plates represented ruptured bubbles walls, but both studies associated these clasts with violent, pulsating, Strombolian activity.

Small (millimeter size) glassy, non-vesicular plates, termed limu o Pele, are observed at lava flow ocean entries and in submarine deposits, notably at Lo’ihi volcano, Hawaii (Schipper and White, 2010). Again, formation models involve the inflation and rupture of basalt bubbles produced by either trapped super-heated seawater (Clague et al., 2000), and/or from magmatic gases associated with Strombolian eruptions (Clague et al., 2003).

CONCEPTUAL MODEL OF FORMATION

We suggest that pajaritos, lava flakes, and the Llaima plates are formed by the same mechanism and recommend the umbrella term “plate tephra” be used to describe similar clasts in the future. Our model elaborates on the basic model invoked by Maleyev and Vande-Kirkov (1983) and accounts for a number of common features of these clasts.

We interpret the distinct shape of the plates, as well as internal textures, as caused by extensional thinning of a magma film originating as walls of large slugs (several to tens of meters in diameter) (Fig. 5a). In this model, expanding bubbles, near or above the vent, experience film thinning, ductile deformation, and then undergo a primary phase of inertial fragmentation, generating large, possibly sheet-shaped tatters of magma. During flight, these ductile tatters are subject to chaotic rotation, torsion, and tension, as well as cooling. Upon cooling to the glass transition temperature and thinning to a critical film thickness of ~4 mm, they fragment brittly forming the observed angular plates. The plates, instead of being ejected ballistically, were entrained into the eruption column and dispersed according to their interaction with the wind field.

Strong crystal alignment during bubble expansion has been reproduced experimentally (Yu et al., 2008). Furthermore, the near perfect crystal alignment with the plate-parallel plane is typically formed in pure shear conditions associated with thinning and extension (Manga, 1998). The observed pinch-and-swell enclaves and flow banding are characteristics inherited at this stage. We infer that initial fragmentation of the bubble film produces fluidal ejecta (on the basis of video observations), so primary fragmentation is inertial, rather than brittle, in nature (Namiki and Manga, 2008). Possible film retraction and additional plastic deformation of these plate parent particles is evident in the form of the surface ridges (i.e., wrinkles, see Debrégeas et al., 1998), variable curvature, tacked edges, and adhered material. The observed cracks are interpreted as tension fracturing of a cooler, brittle crust covering ductile interior. Finally, the abrupt selvages and lack of thinning at the edge of individual plates imply a secondary brittle fragmentation event, probably occurring in the eruption column.

Online videos of the eruption show highly unsteady fire fountaining punctuated by discrete slug bursts occurring tens to hundreds of meters above the vent (Fig. 5a). Illustrative screen shots of footage from 23:00 on 1 January 2008–04:00 on 2 January 2008 (local time) (Figs. 5b and 5c) shows the continued advance and expansion of a fragmentation front populated by large sheets and clots of lava from a recently ruptured slug. In the video, fire fountaining resumes shortly after this particular slug rupture.

IMPLICATIONS

Material Behavior

The plate tephra experience significant rheological changes during the entire formation process. Their complex deformation and fragmentation history is determined by both cooling-related and strain-rate dependent behavior of magma. The limu o Pele have distinctive features (see Schipper and White, 2010), which unlike those of the subaerial plates, are determined by rapid quenching ($10^{5.31}$ K s^{-1}; Potuzak et al., 2008) before fragmentation (i.e., quench granulation; Maicher et al., 2000; Schipper et al., 2013). Calculated minimum quench rates for the Llaima plate tephra range from 2 to 5 K s^{-1} (see the Data Repository), about six orders of magnitude slower than limu o Pele. Thus, initial fragmentation occurs prior to the completion of cooling, allowing for post-fragmentation melt relaxation, plastic deformation, and material adhesion during flight. Assuming the estimated quench rate and an eruption temperature of 1050 °C, the glass transition temperature (700 °C; Gregg and Zimbelman, 2000) could be reached in ~1–3 min, allowing for secondary brittle fragmentation to occur during flight.

Conduit Flow

Magma provenance is inferred from internal textures in the tephra. The high crystallinity and density of the plates and black scoria suggests this magma may have originated near the conduit walls (e.g., Cimarelli et al., 2010), and/or that vesicle collapse occurred during film thinning. The high vesicularity and low crystallinity of the brown scoria suggests a hotter, more volatile-rich magma, that ascended from depth up the center of the conduit.

Video observations indicate highly unsteady eruptive behavior, with intensity and gas decoupling varying on minute to second time scales. The fire fountaining and resultant scoria represent relatively high intensity and either limited gas decoupling (for foam fragmentation), or complete decoupling (if an annular flow regime is achieved). The plates and large slugs indicate periods of relatively low intensity with significant gas decoupling. Rapidly fluctuating behavior is possible due to nonlinear coupling and decoupling of ascending phases (i.e., magma and gas) (Dartevelle and Valentine, 2007), which may be enhanced by viscosity variations in the conduit. According to Pioli et al. (2009), the estimated MER of 10^4 kg s^{-1} implies limited gas decoupling and the development of a sustained column, which corresponds with plume observations (Smithsonian Institution, 2013a). Since MER is an eruption-averaged value, finer scale variations in conduit flow behavior are not captured. In this context plates can be a useful diagnostic feature of highly unsteady violent Strombolian eruptions.

Plume Conditions

Based on their planar shape and similar densities to the scoria, we infer the plates had a lower fall velocity, as a function of increased surface drag and chaotic fall behavior (e.g., tumbling and fluttering) (Foshag and González, 1956; Wilson and Huang, 1979; Andersen et al., 2005; Pioli et al., 2008). This would have allowed increased transport of the plates, with respect to the scoria, which is reflected in the factor of 2.5 difference in the clast diameters at the same distance (Figs. 2a-2c). Further, the cross-wind distribution of plates in the deposit was evidently limited with respect to the scoria; this likely relates to the complex interaction of the plates with the wind field, such as possibly the decoupling from the plume at lower heights.

CONCLUSIONS

We characterize an uncommonly reported type of plate-shaped tephra produced during a violent Strombolian eruption at Llaima volcano. From morphological, textural and video observations we infer the plates are formed by thinning and extension of a magma film, followed by inertial fragmentation as large gas slugs emanate from the conduit and rupture above the vent. The primary fragmentation results in thin sheets that continue to deform in flight, eventually cooling and undergoing secondary, brittle fragmentation to form the observed plates. They are formed during highly unsteady flow where the bursting of discrete gas slugs punctuates the more sustained fire fountaining. The plates are entrained into the eruption column, yet their distinct aerodynamic properties result in slightly modified dispersal features with respect to the scoria. Finally, this class of tephra although not common, is also not unique, and has been briefly described previously under a variety of nomenclature. We propose that these should collectively be termed plate tephra and suggest that they are an important diagnostic feature of the highly unsteady flow conditions common in some violent Strombolian eruptions.

ACKNOWLEDGMENTS

Funding provided by a Geological Society of America Graduate Student Research Grant to Ruth and National Science Foundation grant EAR-0828070 to Calder. Thanks to J. Cortés, D. Schonwalder-Angel, R. Leach, P. Whelley, and A. Brownell for help in the field. Thanks to J. Ball, A. Graettinger, and G. Valentine for helpful discussions. Useful comments were provided by C.I. Schipper and three anonymous reviewers.

REFERENCES CITED

Andersen, A., Pesavento, U., and Wang, Z.J., 2005, Unsteady aerodynamics of fluttering and tumbling plates: Journal of Fluid Mechanics, v. 541, p. 65–90, doi:10.1017/S002211200500594X.

Bonadonna, C., and Costa, A., 2012, Estimating the volume of tephra deposits: A new simple strategy: Geology, v. 40, p. 415–418, doi:10.1130/G32769.1.

Cimarelli, C., Di Traglia, F., and Taddeucci, J., 2010, Basaltic scoria textures from a zoned conduit as precursors to violent Strombolian activity: Geology, v. 38, p. 439–442, doi:10.1130/G30720.1.

Clague, D.A., Davis, A.S., Bischoff, J.L., Dixon, J.E., and Geyer, R., 2000, Lava bubble-wall fragments formed by submarine hydrovolcanic explosions on Lo'ihi Seamount and Kilauea Volcano: Bulletin of Volcanology, v. 61, p. 437–449, doi:10.1007/PL00008910.

Clague, D.A., Batiza, R., Head, J.W., III, and Davis, A.S., 2003, Pyroclastic and hydroclastic deposits on Loihi Seamount, Hawaii, *in* White, J.D.L.,et al., eds., Explosive Subaqueous Volcanism: American Geophysical Union Monograph 140, p. 73–96.

Dartevelle, S., and Valentine, G.A., 2007, Transient multiphase processes during the explosive eruption of basalt through a geothermal borehole (Námafjall, Iceland, 1977) and implications for natural volcanic flows: Journal of Volcanology and Geothermal Research, v. 262, p. 363–384, doi:10.1016/j.epsl.2007.07.053.

Debrégeas, G., de Gennes, P.-G., and Brochard-Wyart, F., 1998, The life and death of "bare" viscous bubbles: Science, v. 279, p. 1704–1707, doi:10.1126/science.279.5357.1704.

Dzierma, Y., and Wehrmann, H., 2010, Eruption time series statistically examined: probabilities of future eruptions at Villarrica and Llaima Volcanoes, Southern Volcanic Zone, Chile: Journal of Volcanology and Geothermal Research, v. 193, p. 82–92, doi:10.1016/j.jvolgeores.2010.03.009.

Foshag, W.F., and González, J., 1956, Birth and development of Parícutin Volcano Mexico: U.S. Geological Survey Bulletin, v. 965, p. 355–489.

Francalanci, L., Tommasini, S., and Conticelli, S., 2004, The volcanic activity of Stromboli in the 1906–1998 A.D. period: mineralogical, geochemical and isotope data relavant to the understanding of the plumbing system: Journal of Volcanology and Geothermal Research, v. 131, p. 179–211, doi:10.1016/S0377-0273(03)00362-7.

Gregg, T.K.P., and Zimbelman, J.R., 2000, Volcanic vestiges, *in* Zimbelman, J.R. and Gregg, T.K.P., eds., Environmental Effects on Volcanic Eruptions: From Deep Oceans to Deep Space: Amsterdam, Kluwer Academin and Plenum Publishers, p. 243–251.

Houghton, B.F., and Wilson, C.J.N., 1989, A vesicularity index for pyroclastic deposits: Bulletin of Volcanology, v. 51, p. 451–462, doi:10.1007/BF01078811.

Maicher, D., White, J.D.L., and Batiza, R., 2000, Sheet hyaloclastite: density-current deposits of quench and bubble-burst fragments from thin, glassy sheet lava flows, Seamount Six, Eastern Pacific Ocean: Marine Geology, v. 171, p. 75–94, doi:10.1016/S0025-3227(00)00109-2.

Maleyev, Y.F., and Vande-Kirkov, Y.V., 1983, Features of pyroclastics of the Northern Breakthrough of the Great Tolbachik Fissure Eruption and the origin of its pale-grey ash, *in* Fedotov, S.A. and Markhinin, Y.K., eds., The Great Tolbachik Fissure Eruption: Geological and geophysical data 1975–1976: Cambridge, UK, Cambridge University Press, p. 57–71.

Manga, M., 1998, Orientation distribution of microlites in obsidian: Journal of Volcanology and Geothermal Research, v. 86, p. 107–115, doi:10.1016/S0377-0273(98)00084-5.

Morgan, D.J., and Jerram, D.A., 2006, On estimating crystal shape for crystal size distribution analysis: Journal of Volcanology and Geothermal Research, v. 154, p. 1–7, doi:10.1016/j.jvolgeores.2005.09.016.

Namiki, A., and Manga, M., 2008, Transition between fragmentation and permeable outgassing of low viscosity magmas: Journal of Volcanology and Geothermal Research, v. 169, p. 48–60, doi:10.1016/j.jvolgeores.2007.07.020.

Pioli, L., Azzopardi, B.J., and Cashman, K.V., 2009, Controls on the explosivity of scoria cone eruptions: Magma segregation at conduit juncitons: Journal of Volcanology and Geothermal Research, v. 186, p. 407–415, doi:10.1016/j.jvolgeores.2009.07.014.

Pioli, L., Erlund, E., Johnson, E., Cashman, K., Wallace, P., Rosi, M., and Delgado Granados, H., 2008, Explosive dynamics of violent Strombolian eruptions: The eruption of Parícutin Volcano 1943–1952 (Mexico): Earth and Planetary Science Letters, v. 271, p. 359–368, doi:10.1016/j.epsl.2008.04.026.

Potuzak, M., Nichols, A.R.L., Dingwell, D.B., and Clague, D.A., 2008, Hyperquenched volcanic glass from Loihi Seamount, Hawaii: Earth and Planetary Science Letters, v. 270, p. 54–62, doi:10.1016/j.epsl.2008.03.018.

Schipper, C.I., Sonder, I., Schmid, A., White, J.D.L., Dürig, T., Zimanowski, B., and Büttner, R., 2013, Vapour dynamics during magma-water interaction experiments: hydromagmatic origins of submarine volcaniclastic particles (limu o Pele): Geophysical Journal International, v. 192, p. 1109–1115, doi:10.1093/gji/ggs099.

Schipper, C.I., and White, J.D.L., 2010, No depth limit to hydrovolcanic limu o Pele: analysis of limu from Lo’ihi Seamount, Hawai’i: Bulletin of Volcanology, v. 72, p. 149–164, doi:10.1007/s00445-009-0315-5.

Institution, S., 2013a, Llaima: Bulletin of the Global Volcanism Network, v. 33, http://www.volcano.si.edu/world/volcano.cfm?vnum=1507-11=&volpage=var#bgvn_3306.

Institution, S., 2013b, Llaima: Bulletin of the Global Volcanism Network, v. 35, http://www.volcano.si.edu/world/volcano.cfm?vnum=1507-11=&volpage=var#bgvn_3506.

Wilson, L., and Huang, T.C., 1979, The influence of shape on the settling velocity of volcanic ash particles: Earth and Planetary Science Letters, v. 44, p. 311–324, doi:10.1016/0012-821X(79)90179-1.

Yu, G., Li, X., Lieber, C.M., and Cao, A., 2008, Nanomaterial-incorporated blown bubble films for large-area aligned nanostructures: Journal of Materials Chemistry, v. 18, p. 728–734, doi:10.1039/b713697h.

Zingg, T., 1935, Beitrage zur Schotteranalyse [Ph.D. thesis]: Zurich, ETH, 141 p.

FIGURE CAPTIONS

Figure 1. A: Location map of Llaima volcano, Chile. B: Southeast view of the eruption plume (~3–5 km above the vent) produced on 15 January 2008. Courtesy of Juan Enrique Llona.

Figure 2. Simplified isopleth maps for plate tephra (A), black (B), and brown (C) scoria. Black dots denote sample locations. Average diameter (cm) was calculated from three measured dimensions of the ten largest clasts at each location, where possible. For the plates, the parenthetical values are the average diameter calculated from the major and intermediate axes only, for easier comparison with scoria isopleths. The insets are the density histograms for each tephra type. Density determined after Houghton and Wilson (1989). D: Deposit isopach map with contours in centimeters.

Figure 3. A: Plot of axial ratios of plates and scoria, the tephra after Wilson and Huang (1979). Note that the plates and scoria fall in separate fields. B: Assorted plates with varied curvature and size. C: Image of curved plate tephra and the major-axis parallel ridges.

Figure 4. A: Thin section image shown parallel to major axis of a plate exhibiting aligned plagioclase and deformed enclaves. B: Backscattered electron (BSE) image of the enclave in A. The plagioclases align around the enclave, which exhibits more Fe-Ti spinel and pyroxene. Image obtained using a SU-70 Hitachi SEM at University at Buffalo, New York, USA. C: Rose diagrams of the main mineral phases. Data plotted in

the northwest quadrant of the rose diagram were projected into the southeast quadrant to obtain the true average orientation. The horizontal axis is 0°. Axial ratios calculated using CSDSlice (Morgan and Jerram, 2006). Additional thin section images are shown in the Data Repository (see footnote 1).

Figure 5. A: Model for plate formation illustrating the relationship between conduit flow and resultant tephra type. B,C: Screen shots of the video at 1:33–1:35. Note, silhouette in the foreground right, corresponds to tree branches. B: Fragmentation front captured after a slug burst. C: Expanding fragmentation front of the same large ruptured slug as in B. Dashed lines in this image show the location of the fragmentation front in B.

[1]GSA Data Repository item 2013xxx, xxxxxxxx, is available online at www.geosociety.org/pubs/ft2013.htm, or on request from editing@geosociety.org or Documents Secretary, GSA, P.O. Box 9140, Boulder, CO 80301, USA.

TABLE 1. DIMENSION DATA FOR 2008–2009 TEPHRA

	n	Average Major Axis (cm)	Average Intermediate Axis (cm)	Average Minor Axis (cm)	Zingg (b/a) (intermediate/major)	Zingg (c/b) (minor/intermediate)
Plates	424	4.5 (±2.4)	3.3 (±1.8)	0.4 (±0.2)	0.7	0.1
Black scoria	1009	3.6 (±1.4)	2.5 (±1.2)	1.6 (±1.1)	0.7	0.6
Brown scoria	1025	2.9 (±1.3)	2.0 (±1.1)	1.3 (±0.8)	0.7	0.7

Note: Numbers in parentheses are 1σ standard deviation and n is number of clasts measured.

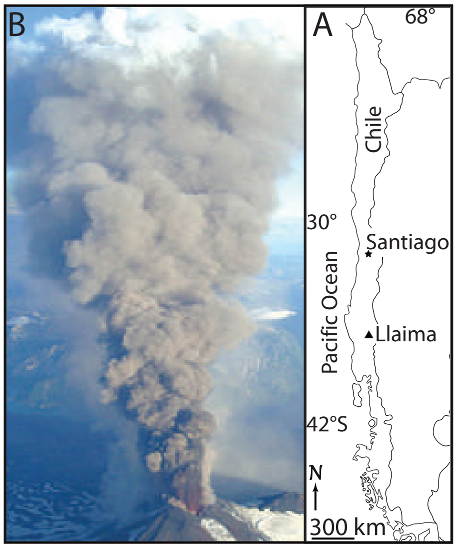

Figure 1

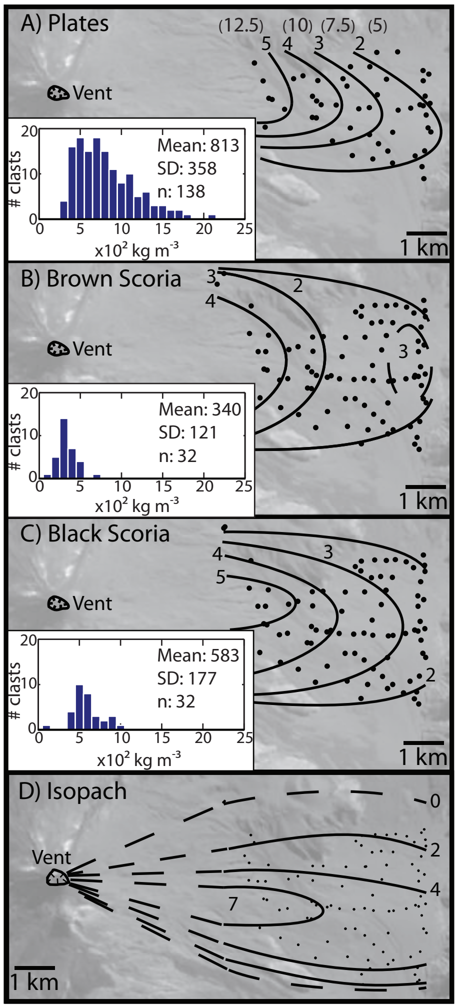

A) Plates
(12.5) (10) (7.5) (5)
5 4 3 2
Vent
Mean: 813
SD: 358
n: 138
clasts
x10² kg m⁻³
1 km
B) Brown Scoria
3
2
4
Vent
Mean: 340
SD: 121
n: 32
1 km
C) Black Scoria
4
3
5
Vent
Mean: 583
SD: 177
n: 32
2
1 km
D) Isopach
0
Vent
2
4
7
1 km

Figure 2

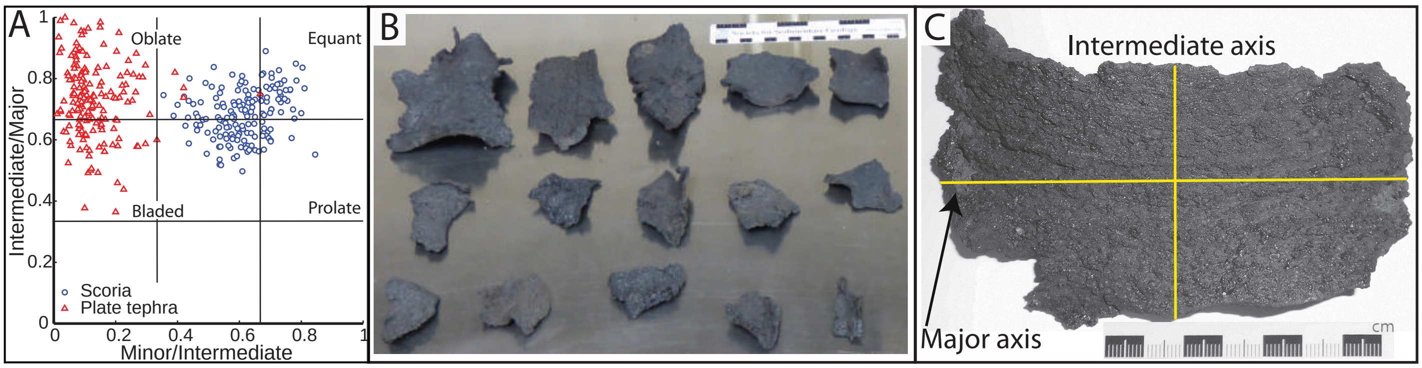
A
Oblate
Equant
Bladed
Prolate
Intermediate/Major
Minor/Intermediate
Scoria
Plate tephra
B
C
Intermediate axis
Major axis
cm

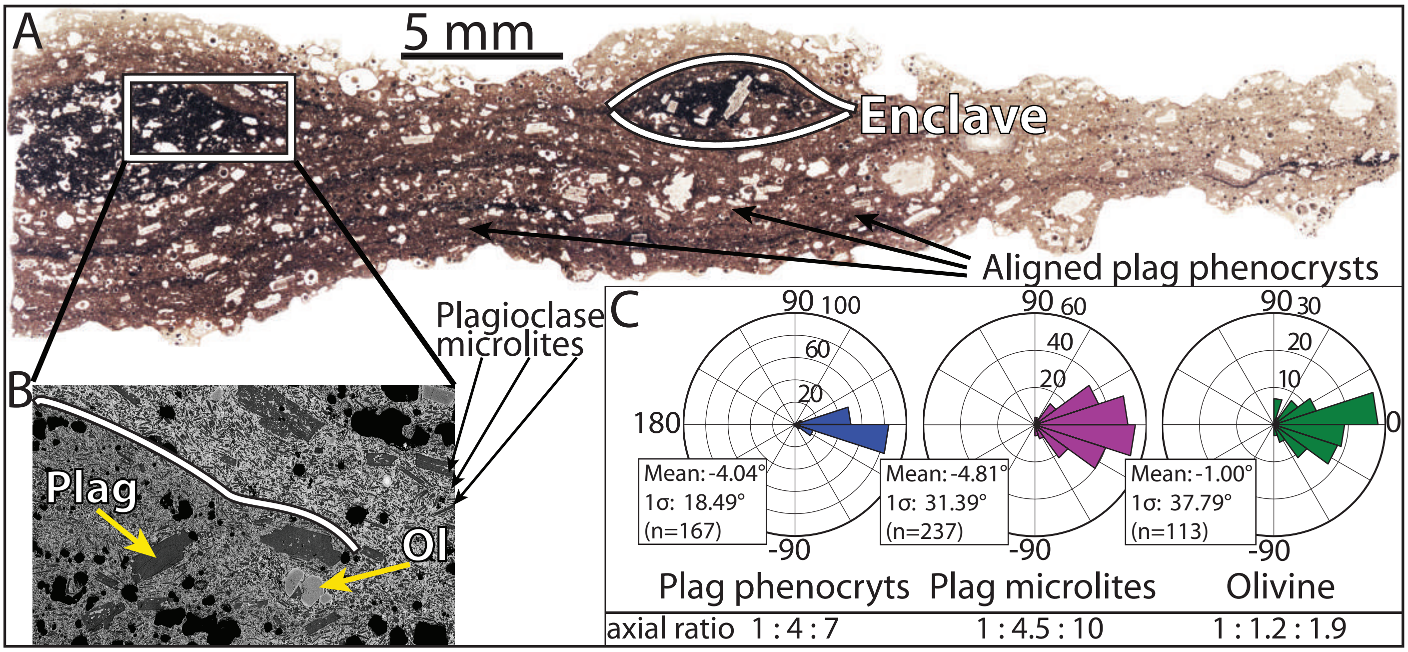
A
5 mm
Enclave
Aligned plag phenocrysts
Plagioclase
microlites
B
Plag
Ol
C
90
100
60
20
180
Mean: -4.04°
1σ: 18.49°
(n=167)
-90
Plag phenocryts
90
60
40
20
Mean: -4.81°
1σ: 31.39°
(n=237)
-90
Plag microlites
90
30
20
10
0
Mean: -1.00°
1σ: 37.79°
(n=113)
-90
Olivine
axial ratio 1 : 4 : 7
1 : 4.5 : 10
1 : 1.2 : 1.9

Figure 4

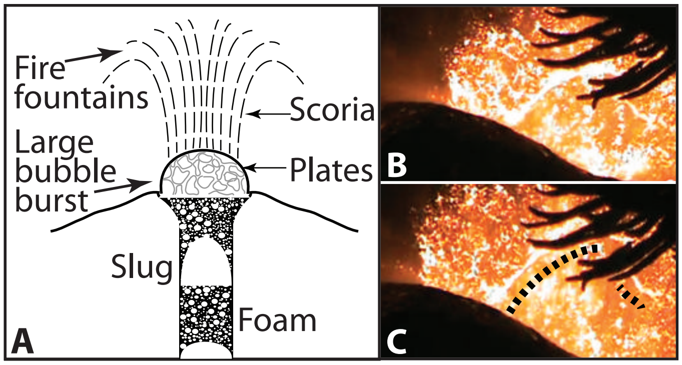
Fire
fountains
Scoria
Large
bubble
burst
Plates
Slug
Foam
A
B
C

Figure 5

SUPPLEMENTAL MATERIALS

Quench rate calculation

Quench rates were estimated using the following equation (Xu and Zhang, 2002):

$$q=(T_{ae}-T_{ff})h/\rho C_p L$$

where T_{ae} is the apparent equilibrium temperature, T_{ff} is the glass transition temperature, h is the heat transfer coefficient, ρ is material density, C_p is the heat capacity of basalt, and L is the effective half thickness of the object (volume/surface area). We assumed an equilibrium temperature of 1450 K, a glass transition temperature of 1000 K (Gregg and Zimbelman, 2000), a heat transfer coefficient of 50 W m^{-2} K^{-1} (Robertson, 1988), a density of 2750 kg m^{-3}, and heat capacity of 1200 J kg^{-1} K^{-1} (Greg and Zimbelman, 2000). To determine L, we assumed the plate shapes were rectangular prisms with the dimensions reported in Table 1.

Figures and Video

Back scattered electron images of the brown and black scoria are provided for reference (Fig. S1). Additional thin sections are provided to show the range of textures observed within the plate tephra (Fig. S2).

Observations of one fragmenting slug concurrent with fire fountaining were conducted on video provided by Patricio Oberg.

References

Gregg, T.K.P., and Zimbelman, J.R., 2000, Volcanic Vestiges, *in* Zimbelman, J.R. and Gregg, T.K.P. eds., Environmental Effects on Volcanic Eruptions: From Deep Oceans to Deep Space, Kluwer Academin/Plenum Publishers, p. 243-251.

Robertson, E.C., 1988, Thermal properties of rocks: U.S. Geologic Survey Open-File Report 88-441, 106 p.

Xu, Z., and Zhang, Y., 2002, Quench rates in air, water, and liquid nitrogen, and inferences of temperature in volcanic eruption columns: Earth and Planetary Science Letters, v. 200, p. 315-330.

FIGURE CAPTION

Figure S1. Back-scattered electron images of brown scoria (A) and black scoria (B). Note that images were collected at the same scale.

Figure S2. An assortment of plate tephra in thin section. All tephra are at approximately the same scale. Note the ubiquitously aligned plagioclase crystals, the presence of flow banding and wide range of vesicularity.

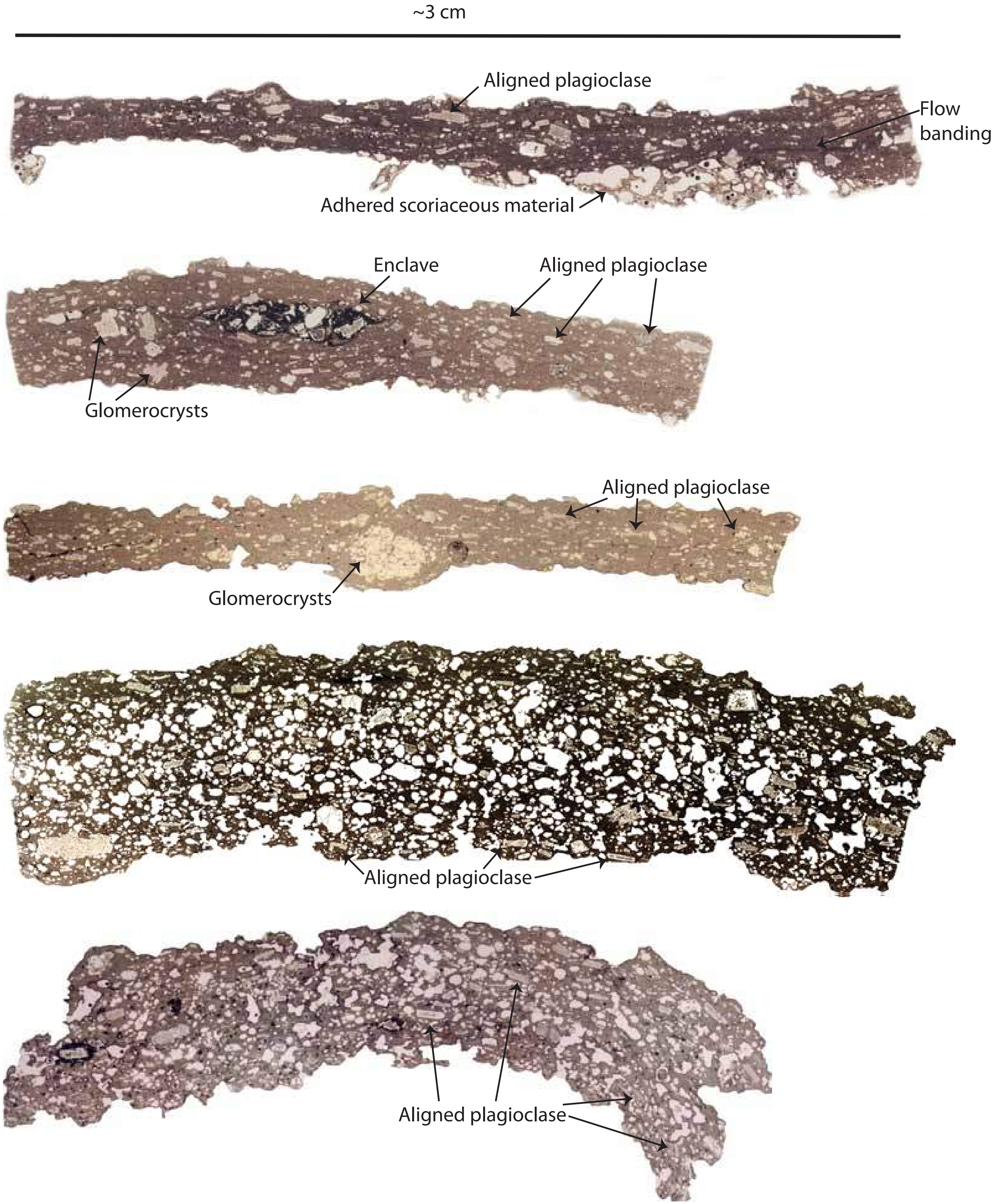

~3 cm
Aligned plagioclase
Flow banding
Adhered scoriaceous material
Enclave
Aligned plagioclase
Glomerocrysts
Aligned plagioclase
Glomerocrysts
Aligned plagioclase
Aligned plagioclase

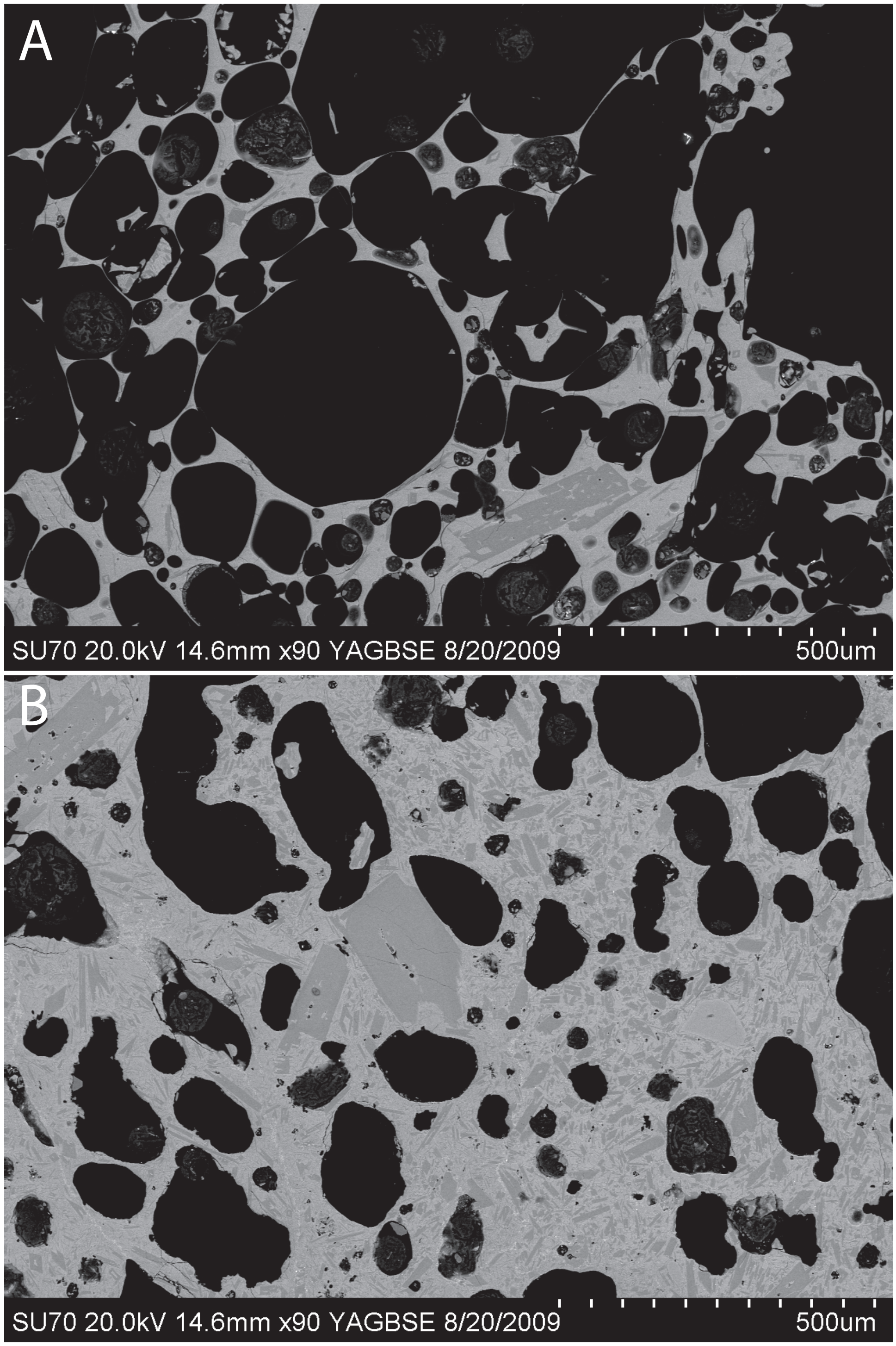
A
SU70 20.0kV 14.6mm x90 YAGBSE 8/20/2009
500um
B
SU70 20.0kV 14.6mm x90 YAGBSE 8/20/2009
500um

Figure S2